J. KAPRA Vol. 10, E(1994) pp. 357-370

Numerical Simulation of Tracer Distribution during CAPTEX

Seung-Bum Kim, Tae-Young Lee

Department of Astronomy and Atmospheric Sciences
and Global Environment Laboratory, Yonsei University
(Received 19 October 1994)

Abstract

This paper introduces an Eulerian long-range transport model coupled with a mesoscale atmospheric model. The model has been applied to the simulation of tracer distribution during two cases of Cross Appalachian Tracer Experiment (CAPTEX). Meteorological fields are predicted by CSU RAMS with four-dimensional assimilation and tracer transport is computed from an Eulerian dispersion model.

The atmospheric model with a four-dimensional assimilation has produced meteorological fields that agree well with observation and has proved its high potential as a generator of meteorological data for a long-range transport model. The present transport model produces reasonable simulations of observed tracer transport, although it was partially successful in the case with complicated structure in observed concentration. Model with Bott's 2nd-order scheme performs as well as that with Bott's 4th-order scheme and increased explicit horizontal diffusivity. Diagnosis of the model results indicates that the present long-range transport model has a good potential as a framework for the acid deposition model with detailed cloud and chemical processes.

1. Introduction

A Long-range air pollutant transport model is a primary tool for studying the source-receptor relationship in the acid deposition problem. It can be classified into two basic types: Lagrangian and Eulerian models. As a basic framework of acid deposition model, the former is used with simpler treatment of atmospheric processes such as chemical transformation and wet and dry deposition, while the latter can accomodate more rigorous treatment of atmospheric processes. The Eulerian model, therefore, can be used with less restriction in actual situation.

There are many existing Eulerian long-range transport models which are developed mostly for the problems in Europe(i.e., Eliassen and Saltbones, 1983) and in North America(i.e, Chang et al., 1987). Some attempts have been reported in recent years for the transboundary transport of air pollutants in the Asian region(i.e., Kotamarthi and Carmichael, 1990; Shim et al., 1993).

Verification of long-range transport model is essential in order to establish the credibility of the model outputs. One of the most popular way of model validation is to simulate the observed tracer transports(i.e., Lee, 1987; Brost et al., 1988). Major data sets for model validation of transport model are mostly available in North America: for example, Across North America Tracer Experiment(ANATEX) (Draxler et al., 1988) and Cross Appalachian Tracer Experiment (CAPTEX) (Ferber et al., 1986). Such data sets, however, are not available for Asian region.

This paper introduces an Eulerian long-range transport model coupled with a mesoscale atmospheric model. The model has been applied to the simulation of tracer transport observed during CAPTEX which consists of 5 cases of tracer (perfluorocarbon(PMCH)) releases from Dayton,

Ohio, the United States and 2 cases of release from Sudbury, Ontario, Canada during the period of mid September through October 1983.

The model is introduced in Section 2, and the performances of atmospheric model and transport model are described in Section 3 followed by summary and conclusions in Section 4.

2. Model

The model consists of a long-range transport model and a mesoscale atmospheric model which provides the necessary meteorological data required for the calculation of transport. Both of these models are written in both Cartesian and polar stereographic coordinate systems, and they are described here in a Cartesian coordinate for simplicity.

2.1 Atmospheric model

A three dimensional hydrostatic model of Colorado State University's Regional Atmospheric Modeling System(CSU RAMS) (Tripoli and Cotton, 1982; Tremback et al., 1985) is employed as the atmospheric model.

2.1.1 Governing equations

Equation of motion on a sigma-z coordinate can be written as

$$\frac{\partial \overline{u_1}}{\partial t}+\overline{\theta}\frac{1}{a}\left[\frac{\partial(a b^{1j}\overline{\Pi})}{\partial x_j^*}\right] = ADV(\overline{u_1})+TURB(\overline{u_1})+f\overline{u_2} \quad \cdots\cdots(1)$$

$$\frac{\partial \overline{u_2}}{\partial t}+\overline{\theta}\frac{1}{a}\left[\frac{\partial(a b^{2j}\overline{\Pi})}{\partial x_j^*}\right] = ADV(\overline{u_2})+TURB(\overline{u_2})-f\overline{u_1} \quad \cdots\cdots(2)$$

where $\overline{u_1}$ and $\overline{u_2}$ represent the wind speeds in x and y directions, respecitively, $\overline{\theta}$ the potential temperature, $a=1-\frac{z_s}{H}$, z_s the height of ground surface, H the height of model top, b^{ij} the tensor for coordinate transformation, f the Coriolis parameter, Π the Exner function$(=c_p(\frac{p}{p_0})^{\frac{R_d}{c_p}})$, c_p the specific heat at constant pressure, p the pressure, p_0 the reference pressure (1000hpa), R_d the gas constant for dry air, ADV and $TURB$ are operators for advection and turbulent diffusion, respectively, which are defined as

$$ADV(\overline{A})= -\frac{1}{\rho_0 a}\left[\frac{\partial(a b^{jk}\rho_0 \overline{u_j}\,\overline{A})}{\partial x_k^*}-\overline{A}\frac{(a b^{jk}\rho_0 \overline{u_j})}{\partial x_k^*}\right],\ j,\ k=1,2,3 \quad \cdots\cdots(3)$$

$$TURB(\overline{A})= -\frac{1}{a}\frac{\partial[a b^{jk}(\overline{A''u_j''})]}{\partial x_k^*},\ j,k=1,2,3 \quad \cdots\cdots(4)$$

where ρ_0 is the reference state density and $\overline{u_3}$ represents the vertical velocity.

Anelastic continuity equation is written as

$$\frac{1}{a}\frac{\partial(a b^{ij}\overline{\rho}\,\overline{u_j})}{\partial x_j^*}=0,\ ij=1,2,3 \quad \cdots\cdots(5)$$

Thermodynamic equation is written as

$$\frac{\partial(\overline{\theta})}{\partial t}=ADV(\overline{\theta})+TURB(\overline{\theta}) \quad \cdots\cdots(6)$$

Hydrostatic equation is written as

$$\frac{\partial \overline{\Pi}}{\partial z^*}=-a\frac{g}{\overline{\theta}_v} \quad \cdots\cdots(7)$$

where g is the gravity and $\overline{\theta}_v$ is the virtual potential temperature.

2.1.2 Parameterization

Turbulence exchange for variable $A\,(\overline{A''u_j''})$ is parameterized using the first-order closure method for which the following form of exchange coefficient is used :

$$K_m=\frac{c^2}{\sqrt{2}}\,l^2\,|\,D^2\,|\,(1-\frac{K_h}{K_m}Ri)^{1/2} \quad \cdots\cdots(8)$$

$$K_h=3K_m \quad \cdots\cdots(9)$$

where K_m and K_h are the exchange coefficients for momentum and heat, respectively, l the turbulence scale length, D the deformation, c a constant, and Ri is the Richardson number.

Temperature and moisture at ground surface are predicted using the method of Tremback and Kessler(1985).

2.1.3 Numerical methods

The model uses C-staggered grid system

(Mesinger and Arakawa, 1976) in which all thermodynamic and tracer variables are located at the center while the velocity components $\overline{u_1}$, $\overline{u_2}$, $\overline{u_3}$ are placed $1/2\Delta_x$, $1/2\Delta_y$, $1/2\Delta_z$, respectively. A second-order finite difference method is used for spatial derivatives.

Davies(1976) nudging condition is used for lateral boundaries and prognostic surface pressure method is used for upper boundary condition in which horizontal divergence is assumed to be zero above the model top.

2.1.4 Initialization and four-dimensional assimilation

Initial and consecutive 12 hourly reference fields are obtained from ECMWF data sets using an isentropic analysis package of CSU RAMS. Objective analysis method of Barnes(1964) is used.

A four-dimensional assimilation technique is added to the CSU RAMS for meteorological prediction. The technique used in this study known as Newtonian relaxation or "nudging" (Kistler, 1974; Anthes et al., 1974). The relaxation terms, $k(A_R - A)$ have been added to the prognostic equations for $A=(\overline{u}_1, \overline{u}_2, \overline{\theta})$. The reference fields A_R are obtained from the 12 hourly analysed upper atmospheric fields through linear temporal interpolation. In this experiment, the wind and temperature fields are assimilated everywhere except that the temperature is not assimilated inside the PBL in order to include its diurnal variation. Moderate nudging ($k = 10^{-4}s^{-1}$) is used.

2.2 Transport model

2.2.1 Dispersion equation

A three-dimensional Eulerian dispersion equation on a sigma-z coordinate may be written as

$$\frac{\partial \bar{c}}{\partial t} = ADV(\bar{c}) + \left[\frac{H}{H - z_s}\right]^2 \frac{\partial}{\partial z^*}\left[K_c \frac{\partial \bar{c}}{\partial z^*}\right] + Q + R \quad \cdots\cdots(10)$$

where $\bar{c}$ is the tracer concentration, K_c the eddy exchange coefficient for atmospheric pollutant, Q the source term, and R is the chemical reaction term. The advective operator is the same as in (3). The source term and chemical reaction term are neglected in the present study. The wind speeds and eddy exchange coefficient are provided by the atmospheric model. The eddy exchange coefficient for pollutant(K_c) is assumed to be identical to that for heat(K_h)((8) and (9)).

2.2.2 Numerical methods

Concentration is placed at the center of a grid where thermodynamic variables are located. An explicit forward difference method is used for time differencing, except for vertical diffusion in which an implicit method is employed.

Four positive definite schemes have been initially considered to treat the horizontal advection of pollutant: 2nd-and 4th-order schemes of Bott(1989, 1992), Smolarkiewicz(1983) scheme, Prather (1986) scheme. These schemes are applied to the advection of cone on the cylinder shaped tracer distribution in a rotational flow field(Fig. 1). The results after six rotations are shown in Fig. 2.

The Prather scheme performs best while the Smolarkiewicz scheme performs worst. Model performances in these experiments are quantitatively evaluated by comparing the values for peak concentration ratio($c_{max}(t)/c_{max}(0)$), mass conservation ratio ($\sum c(t)/\sum c(0)$) and mass distribution ratio($\sum c^2(t)/\sum c^2(0)$). These values for the four schemes are given in Table 1.

(a)

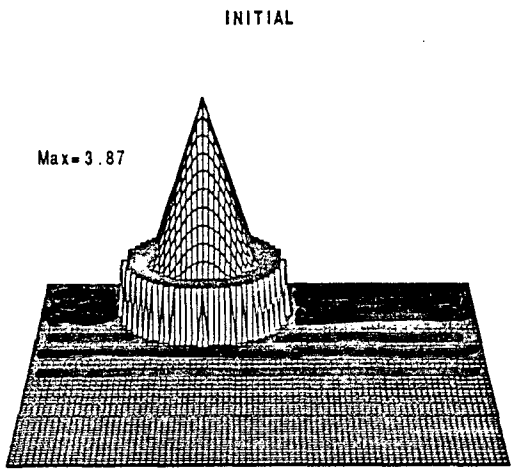

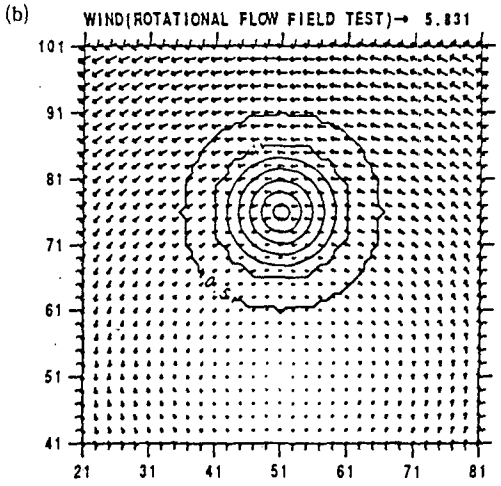

Fig. 1. (a) Initial shape of concentration distribution and (b) the rotational flow fields.

The Prather scheme shows the best performance in all aspects and the Bott's 4th-order scheme performs as good as the Prather scheme. Bott's 2nd-order scheme also performs well conserving mass except the lowering of maximum concentration which may be due to numerical diffusion. The Smolarkiewicz scheme gives the poorest performance on conservation and distribution of mass and the location of maximum concentration. The CPU time for computation required by Prather scheme is about 6, 2.3, 3 times larger than those of Bott's 2nd-order, Bott's 4th-order and Smolarkiewicz schemes, respectively.

According to Brost et al.(1988), an explicit horizontal diffusion may be required for the simulation of tracer transport when a model uses scheme with small numerical diffusion such as Prather scheme

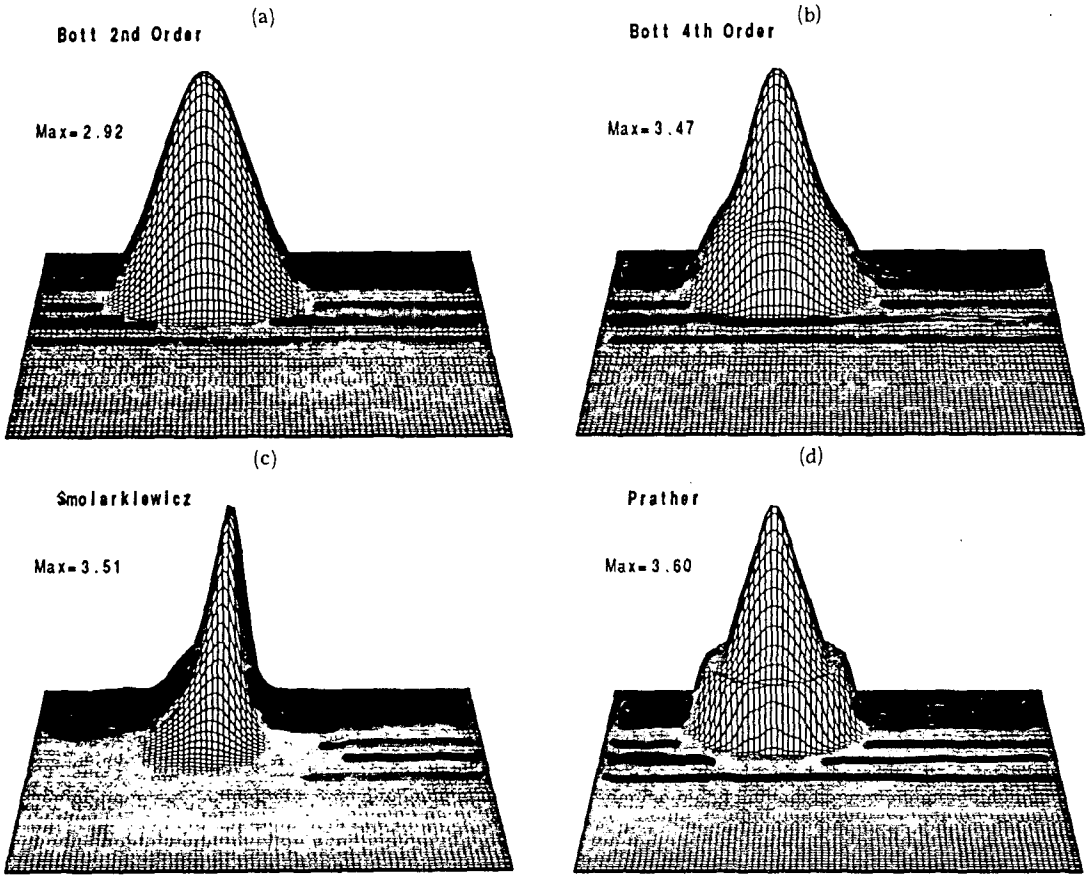

Fig. 2. Results after six rotations by (a) Bott's second-order, (b) Bott's fourth-order, (c) Smolarkiewicz and (d) Prather schemes.

Table 1. Peak concentration ratio($c_{max}(t)/c_{max}(0)$), mass conservation ratio ($\sum c(t)/\sum c(0)$), mass distribution ratio($\sum c^2(t)/\sum c^2(0)$) and location of maximum concentration obtained from the results after six rotations.

Schemes	$\frac{c_{max}(t)}{c_{max}(0)}$	$\frac{\sum c(t)}{\sum c(0)}$	$\frac{\sum c^2(t)}{\sum c^2(0)}$	Location of maximum concentration (51,76)
Bott's 2nd	0.76	1.00	0.91	(52,76)
Bott's 4th	0.90	1.00	0.96	(51,76)
Smolarkiewicz	0.91	0.85	0.78	(56,76)
Prather	0.93	1.00	0.97	(51,76)

and Bott's 4th-order scheme. In this respect, the numerical diffusion of Bott's 2nd-order scheme may well be accepted for actual application. Since the two schemes of Bott(1989, 1992) perform almost as good as the Prather's scheme with much less computation time except for numerical diffusion of 2nd-order scheme, we use them in the simulation of CAPTEX tracer transport and evaluate them further.

The concentrations at the upstream boundaries are assumed to be zero and zero gradient condition is used for downstream boundaries in this study. No pollutant flux through ground surface is assumed.

3. Simulation of tracer transport

The model is applied to the simulation of tracer distribution during two cases of CAPTEX(Ferber et al., 1986). The cases treated here are the first (CAPTEX 1) and second (CAPTEX 2) releases among 7 releases of CAPTEX. In CAPTEX 1, 208kg of tracer(PMCH) is released during the three-hour period of 1700-2000 UTC 18 September 1983 at Dayton (39.80 °N, 84.05 °W), Ohio in the United States. In CAPEX 2, 201kg of tracer is released at Dayton during 1705-2005 UTC 25 September 1983.

The numerical integration starts about 5 hours before the start of tracer release, and is carried out for 36 hours for CAPTEX 1 and 48 hours for CAPTEX 2 in a domain of 3500km×2870km×15km with uniform horizontal grid size of 70km. Time step is 120 seconds. Tracer is released at the location of Dayton, Ohio for three hours with the rates of 19.26g/s and 18.61g/s for CAPTEX 1 and CAPTEX 2, respectively.

3.1 Meteorological fields

In this section, we will present the simulated meteorological fields and compare them with observation only for CAPTEX 1 because the comparison obtained in CAPTEX 1 similarly applies to the case of CAPTEX 2.

In CAPTEX 1, low pressure systems are initially over the northwest and northeast of the model domain and a minor high pressure area is located over the southeast of the release point(marked by ⊠) (Fig. 3). Lower level winds near the release point is generally in between southwesterly and westerly. The wind speeds at $z^*=1253$m are stronger than those at low level although the flow patterns are similar.

Predicted meteorological fields for 12UTC 19 September 1983(24 hour of integration) are compared with observations in Fig. 4 and 5. Observed fields are obtained from the ECMWF data using an isentropic analysis package in CSU RAMS which uses Barnes(1964) type objective analysis technique. Sea-level pressure patterns agree very well with observation. The pressure systems generally have moved eastward. Winds near the release point become southwesterly at both levels of $z^*=90$m and 1253m. Predicted fields agree very well with the observations.

Root mean square errors(RMSE) of predicted meteorological fields are obtained from the simulated and observed fields and are listed in Table 2. RMSE for wind vectors includes both the errors in direction and speed. RMSE decreases with height

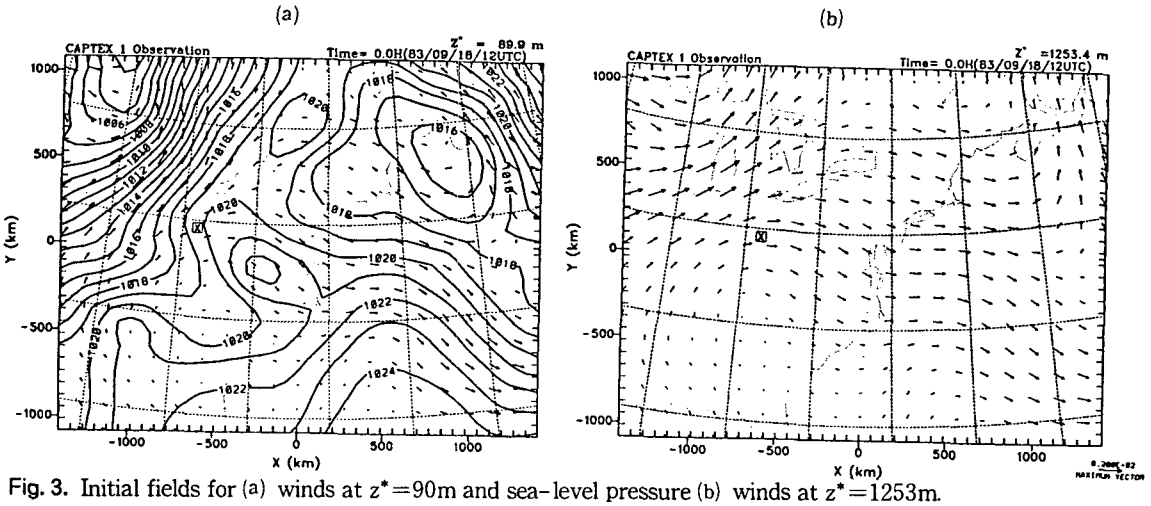

Fig. 3. Initial fields for (a) winds at $z^*=90$m and sea-level pressure (b) winds at $z^*=1253$m.

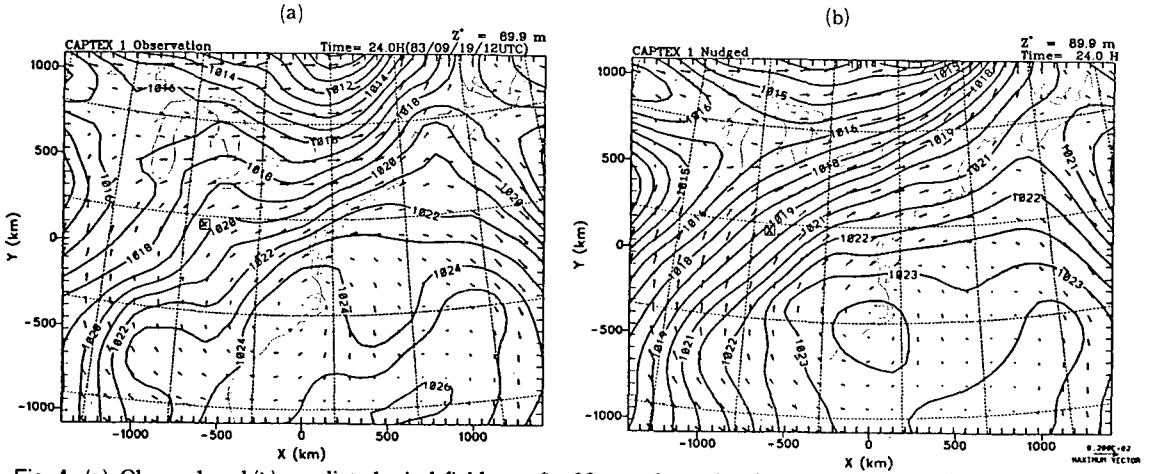

Fig. 4. (a) Obseved and (b) predicted wind fields at $z^*=90$m and sea-level pressure at 12UTC September 19, 1983.

Table 2. Root mean square error of predicted meteorological fields for CAPTEX 1.

	RMSE-V(m/s)			RMSE-T(K)			RMSE-Ps(hPa)
z^*(m)	90	702	2080	90	702	2080	sea-level
12 hour	1.4	1.4	1.0	2.4	1.0	0.6	1.6
24 hour	1.4	1.2	1.1	1.9	0.7	0.7	2.1
36 hour	1.3	1.2	0.8	2.7	1.3	0.7	2.4

and its values are in the range of 1.2-1.4 m/s at the levels of z^* = 90 and 702m and 0.8-1.1 m/s at the level of z^* = 2080m which is above the PBL top. The magnitudes of these values are similar to those of errors in analysed meteorological fields. The RMSE for sea-level pressure which is not assimilated is increasing with time from 1.6 hPa at 12 hour to 2.4 hPa at 36 hour of integration. The use of nudging seems quite successful according to these results.

3.2 Tracer transports

Various numerical experiments have been performed for the two CAPTEX cases to investigate the model performance and its dependence on numerical schemes, magnitude of horizontal diffusion, and vertical resolution in PBL(Table 3). Experi-

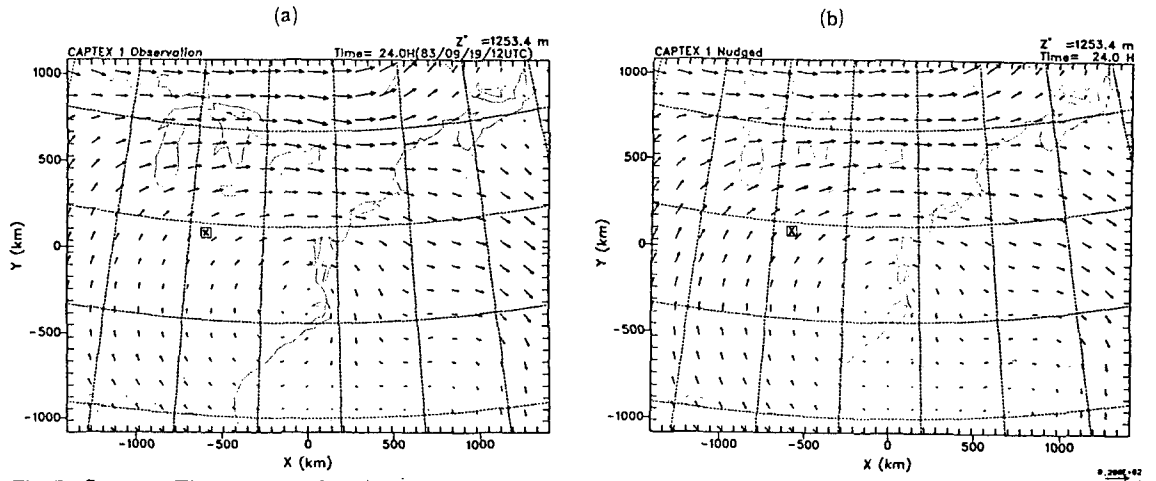

Fig. 5. Same as Fig. 4, except for $z^*=1253$m.

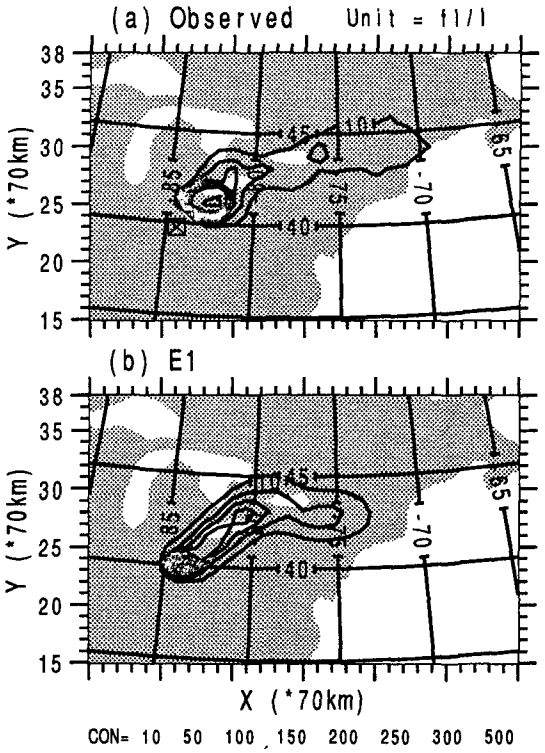

Fig. 6. Comparison of (a) observed plume with (b) predicted plume from the experiment E1 for CAPTEX 1. The number at the bottom indicates the value for each contour line.

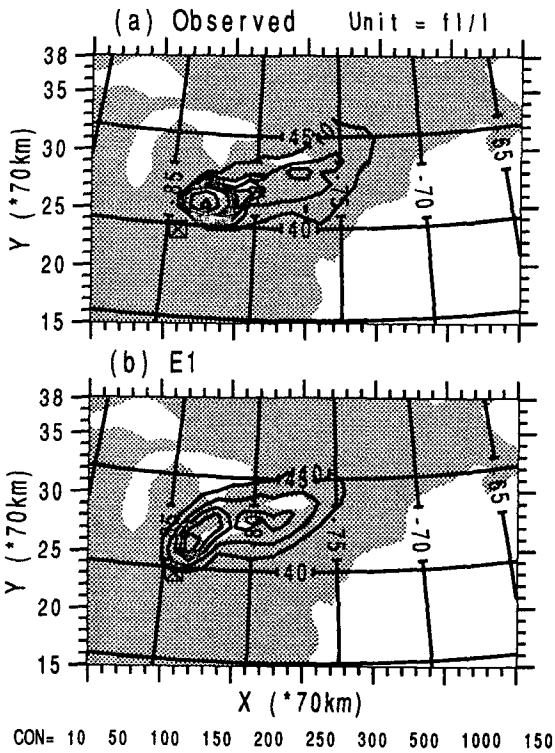

Fig. 7 Same as Fig. 6, except for CAPTEX 2.

ments E1 and E2 are to evaluate the performance with Bott's 4th- and 2nd-order schemes, respectively, E3 and E4 are to see the variation of performance with different values of horizontal exchange coefficient. E5 is to see the effect of higher vertical resolution in PBL.

3.2.1 Tracer transports

Each release of tracer during 3-hour period was followed by four consecutive sampling periods of 6-h integrated samples. The four periods for CA-

Table 3. Summary of numerical experiments.

	Numerical Scheme	Horizontal Diffusion (m^2s^{-1})	PBL Resolution
E1	Bott's 4th	10^4	Lower
E2	Bott's 2nd	10^4	Lower
E3	Bott's 4th	0	Lower
E4	Bott's 4th	3.3×10^4	Lower
E5	Bott's 4th	10^4	Higher

PTEX 1 are 7-13 hour(19UTC 18 September-01UTC 19 September), 13-19 hour(01-07UTC 19 September), 19-25 hour(07-13UTC 19 September) and 25-31 hour(13-19UTC 19 September) of integration. For CAPTEX 2, those are 15-21(03-09UTC 26 September), 21-27 hour(09-15UTC 26 September), 27-33 hour(15-21UTC 26 September), 33-39 hour(21UTC 26 September-03UTC 27 September). Predicted tracer distributions are presented in terms of "puff" and "event-total plume".

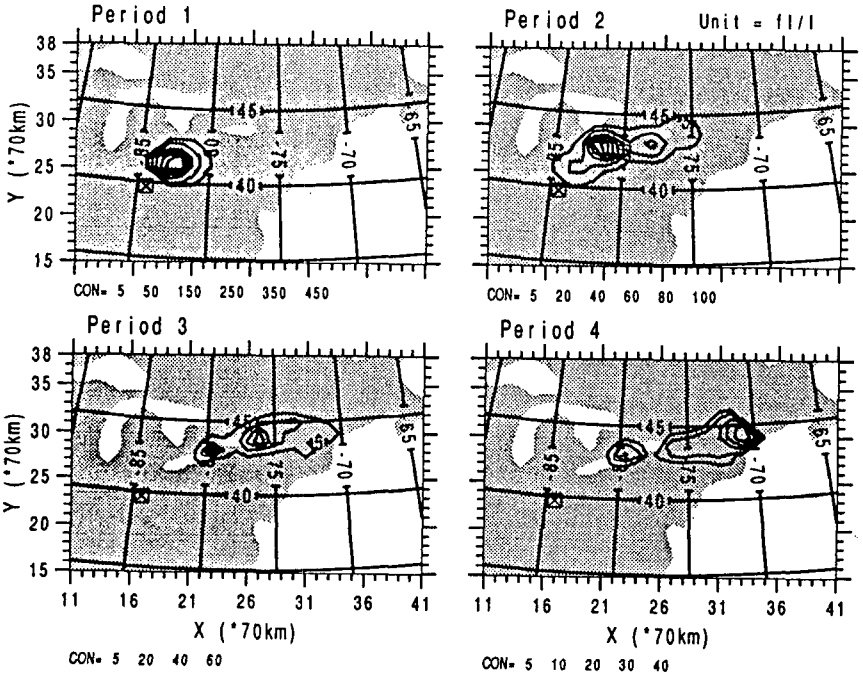

Fig. 8. Observed puffs for the four periods in CAPTEX 1.

Hereafter, a puff is defined by the isopleths of concentration for an individual 6-h data period and an event-total plume is defined by the maximum concentration during the whole period at the first grid level above ground.

Simulated plume from E1 experiment is shown with the observed plume for CAPTEX 1(Fig. 6) and CAPTEX 2(Fig. 7). The observed plume for CAPTEX 1 elongates northeastward near the release point and then nearly eastward extending to the east coast(Fig. 6a). The concentration decreases rapidly from the point of maximum concentration. The predicted plume is also similarly elongated except that the eastern part of the plume is somewhat south of the observed plume and does not reach the east coast. There was no surface observation site close to the release point and that may explain why the observed plume starts somewhat downstream side of the release point. The difference in the extension of the plume to the east coast is more difficult to explain and will be addressed later in description of simulated puffs. Another discrepancy is that the simulated concentration is much higher in the eastern part of the plume. This may be related to the weak horizontal and vertical diffusion.

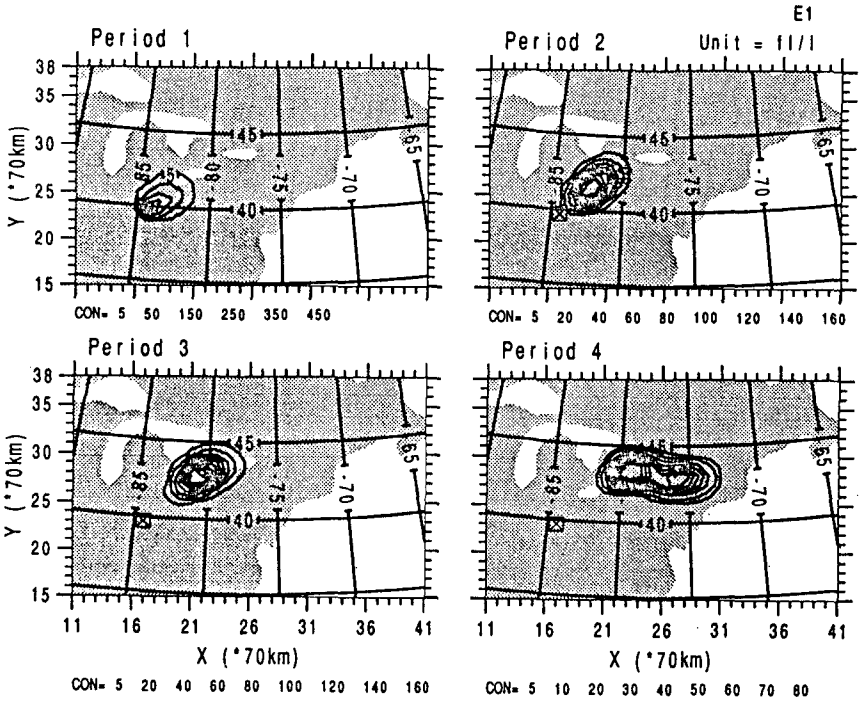

Fig. 9. Predicted puffs for the four periods in CATPEX 1. The puffs are from the experiment E1.

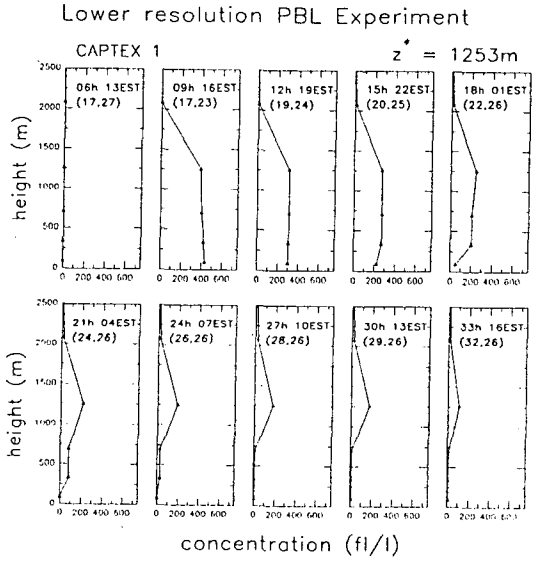

Fig. 10. Vertical distribution of simulated tracer concentration following the location of maximum concentration at the level of z^* =1253m from experiment E1 for CAPTEX 1. The number in the parenthesis represent the location of grid point (i_x, j_y).

The observed plume in CAPTEX 2 is shorter but wider than that in CAPTEX 1. In this case, the agreement between observation and simulation is fairly good in various aspects such as the size and direction of plume and concentration within plume.

Observed puffs in CAPTEX 1 are shown in Fig. 8. These puffs are obtained from the observed surface concentration by the Cressman-type interpolation technique. The observed puff moves northeastward passing the lakes Erie and Ontario during the first and second periods and eastward in the last two periods. The puff shows complicated structure from the second periods with two maxima of concentration. The concentration within puff is decreasing with time.

Predicted puffs(Fig. 9) move northeastward crossing Lakes Erie and Ontario during the first three periods and then eastward during the last period. The simulation agrees partially with observation mainly due to the failure of simulating the double maximum structure observed in the periods 2 and 3.

One possible explanation for the failure of simulating the double maxima structure may be due to the failure in proper simulation of the effects of

vertical shear of wind and turbulent diffusion. Pollutant transported to higher level may be transported by stronger wind farther downstream ahead of the surface maximum and can be transported downward by turbulence. This reasoning may be supported by the Fig. 10 which shows the vertical distribution of simulated concentration following the location of maximum concentration at the level of $z^*=1253$m for CAPTEX 1. At 9h(16 EST 18 September), the tracer is vertically well mixed. The concentration at lower level decreases toward nighttime mainly because of wind shear which can cause the tracer at higher and lower levels to move with different velocities. Tracer at $z^*=1253$m is moving without any downward mixing during nighttime and has moved to the grid point (29,26) at 30h(13 EST 19 September) which is near the east coast and is about 157km southeast of the location of surface maximum concentration. But the pollutant at this level is still not mixed downward in the daytime of the second day due to negligible turbulent exchange.

Another major difference between the observed and simulated puffs for CAPTEX 1 is in the concentration value. The simulated puffs shows higher concentration especially in the later periods. Similar difference is already pointed out in the comparison of observed and simulated plumes(Fig. 6).

Observed puffs in CAPTEX 2 show less elongated structure than those of CAPTEX 1(Fig. 11). The agreement between observation and simulation is fairly good through the periods except for the period 2 when the observation shows a elongated structure with double maxima(Fig. 12). The value of concentration within puffs compare well with observation in this case. The vertical profile of simulated concentration following the location of maximum concentration at $z^*=1253$m is shown in Fig. 13. In this CAPTEX 2, the tracer at the upper layer of PBL is mixed downward as the PBL top ascends in the second day.

3. 2. 2 *Quantitative evaluation of model performance*

Quantitative evaluation of model performance is carried out by calculating three scores (bias, threat and overlap scores), trajectory error, and ratio of simulated maximum concentration to

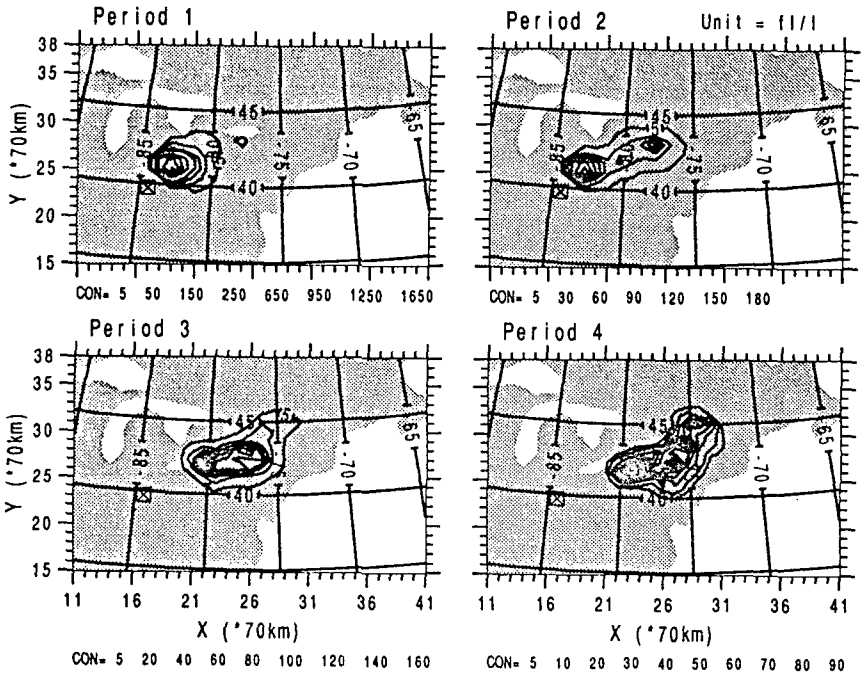

Fig. 11. Same as Fig. 8, except for CAPTEX 2.

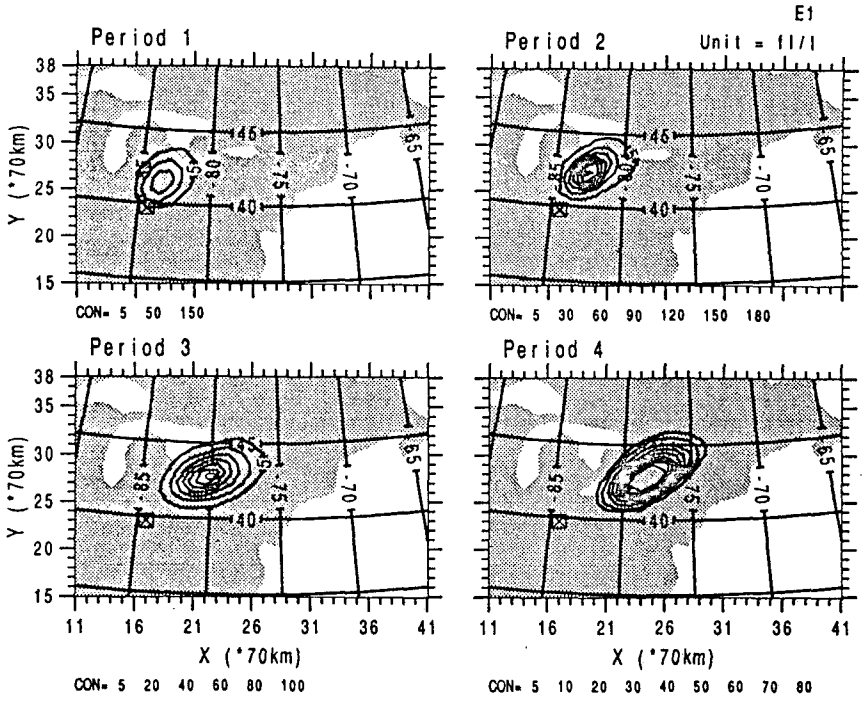

Fig. 12. Same as Fig. 9, except for CAPTEX 2.

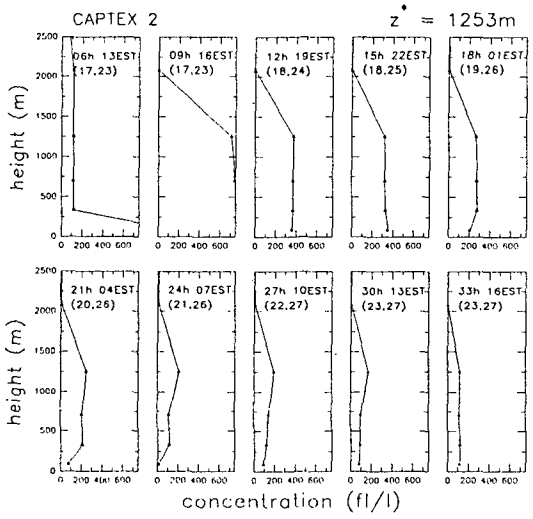

Fig. 13. Same as Fig. 10, except for CAPTEX 2.

observed maximum concentration.

(a) Scores

Three different sizes of puff are considered for the calculation of scores : puffs are defined by the region with concentration greater than 1, 10 and

Table 4. The three scores for each experiment for three different threshold values defining puff in CAPTEX 1. The score represents average value for the two periods 2 and 3.

	E1	E2	E3	E4	E5
		Bias Score*			
1%	0.54	0.69	0.49	0.63	0.50
10%	0.68	0.85	0.64	0.74	0.59
50%	1.58	2.05	1.45	1.58	1.25
		Threat Score**			
1%	0.32	0.34	0.30	0.34	0.29
10%	0.25	0.26	0.25	0.26	0.23
50%	0.15	0.13	0.16	0.15	0.06
		Overlap Score***			
1%	0.36	0.42	0.34	0.41	0.33
10%	0.30	0.34	0.30	0.32	0.27
50%	0.33	0.33	0.33	0.33	0.10

* Bias score=FA/OA

** Threat score=CFA/(OA+FA−CFA)

***Overlap score=CFA/OA

※FA : Forecasted area, OA : Observed area, CFA : Correctly forecasted area

Table 5. Same as Table 4, except for CAPTEX 2.

	E1	E2	E3	E4	E5
		Bias Score			
1%	0.78	1.02	0.69	1.06	0.75
10%	1.04	1.30	0.94	1.30	0.99
50%	1.02	1.28	0.91	1.22	1.06
		Threat Score			
1%	0.37	0.39	0.35	0.39	0.36
10%	0.27	0.31	0.27	0.30	0.29
50%	0.10	0.19	0.08	0.17	0.20
		Overlap Score			
1%	0.49	0.57	0.43	0.58	0.47
10%	0.43	0.54	0.42	0.54	0.44
50%	0.18	0.33	0.13	0.31	0.33

50% of maximum concentration within puff. Tables 4 and 5 show the scores of the five experiments for CAPTEX 1 and 2, respectively.

In CAPTEX 1, the bias scores, which is a measure of agreement in size of puff, indicate that the size of simulated puff, is generally smaller than that of observed puff. This may be understandable when we consider the fact that the concentration in simulated puff is larger than that in observation. This score is larger with Bott's 2nd-order scheme (E2) than with Bott's 4th-order scheme(E1), and increases as the magnitude of explicit horizontal diffusion increases. In CAPTEX 2, the bias score is larger than that for CAPTEX 1 showing values around 1.

The threat and overlap scores give a measure of the coincidence of simulated puff with observed puff. The threat score may be a better indicator for the model performance, because the overlap score can increase toward 1 when the simulated puff becomes larger. The variation of threat score with experiment is not very large in both cases. Threat scores also indicate that the enhancement of vertical resolution in PBL does not necessarily improve the simulation, but the increase of horizontal diffusion somewhat improves score. E2 and E4 produce the highest score in both CAPTEX cases. As the puff threshold value increases, the score decreases for all experiments of two cases. Dependence of score on experiments in CAPTEX 2 is similar to that for CAPTEX 1.

(b) Trajectory error and maximum concentration ratio

Average trajectory error and maximum concentration ratio (simulated maximum concentration/observed maximum concentration) are listed in Tables 6 and 7. The values are average over periods 2 and 3. Trajectory error is the distance between grids of observed and simulated maximum concentration over the periods 2 and 3. The five experiments produce similar trajectory errors, although E2 shows smaller error on the average.

The ratio shows some difference between CAPTEX 1 and 2. It is in the range of 1.55-2.17 for CAPTEX 1 and 0.66-0.95 for CAPTEX 2. The two case average ratio is 1.43 for E1, 1.11 for E2 and 1.19 for E4. These results reflect the effects on the maximum concentration by numerical diffusion of Bott's 2nd-order scheme(E2) and by the increase of explicit horizontal diffusion(E4).

Table 6. Trajectory error*(e_T, km) and ratio*(b) of simulated maximum concentration to observed maximum concentration during periods 2 and 3 for CAPTEX 1.

	E1	E2	E3	E4	E5
e_T	113	113	113	113	157
b	2.02	1.55	2.17	1.72	2.16

* Averaged value for period 2 and 3

Table 7. Same as Table 6, except for CAPTEX 2.

	E1	E2	E3	E4	E5
e_T	140	105	140	140	105
b	0.83	0.66	0.93	0.66	0.95

(c) Discussions

Some common dependencies of model performance on the numerical schemes, magnitude of horizontal diffusion may be found from the results of numerical experiments for the two cases of CAPTEX, although the variations of scores, trajectory error and maximum concentration ratio with experiment are not very large. Model with Bott's 2nd-order scheme(E2) produces very similar results to those of Bott's 4th-order scheme with explicit horizontal diffusion of 3.3×10^4 m^2s^{-1}(E4).

And these two experiments produce highest threat score. The effect of numerical diffusion of Bott's 2nd-order scheme seems comparable to the effect of increased explicit horizontal diffusion from 10^4 to 3.3×10^4 m^2s^{-1} which improved the result with Bott's 4th-order scheme.

Increase of explicit horizontal diffusion somewhat improves the scores but it does not change the trajectory error. The two cases show different performance changes as the vertical resolution in the lower atmosphere increases and the impacts of vertical resolution are not clear according to these results.

The present results indicate that Bott's 2nd-order scheme may be used instead of 4th-order scheme. Further study is necessary, however, to derive conclusion of the model dependence on various model factors with larger amount of validation data sets.

4. Summary and Conclusions

A long-range transport model has been developed and applied to the simulation of tracer distribution during two cases of CAPTEX. In this study, the meteorological fields are predicted by CSU RAMS with four-dimensional assimilation and tracer transport is computed from an Eulerian transport model.

The atmospheric model of CSU RAMS with a four-dimensional assimilation has produced meteorological fields that agree well with observation and has proved its high potential as a generator of meteorological data for a long-range transport model. The present transport model produces reasonable simulations of observed tracer transport, although it was partially successful in the case with complicated structure in observed concentration. Model with Bott's 2nd-order scheme performs as well as that with Bott's 4th-order scheme and increased explicit horizontal diffusivity.

Diagnosis of the model results indicate that the present long-range transport model can be further improved and has a good potential as a framework for the acid deposition model with detailed cloud and chemical processes. Improvement in treatment of vertical diffusion seems important for the improvement of model performance.

(Acknowledgements)

This paper is a part of the results from Research and Development on Technology for Monitoring and Prediction of Acid Rain which is supported by the Ministry of Environment and the Ministry of Science and Technology through the G7 project on Research and Development on Technology for Global Environmental Monitoring and Climate Change Prediction.

References

Anthes, R. A., N. Seaman, J. Sobel, and T. Warner (1974) The development of mesoscale models suitable for air pollution studies, Select Group in Air Pollution Meteorology, Second Annual Progress Report, Vol. 1, Environmental Protection Agency, Research Triangle Park, N. C. 27711, 271pp.

Barnes, S.(1964) A technique for maximizing details in numerical map analysis, J. Appl. Meteor., 3, 395-409.

Bott, A.(1989) A positive definite advection scheme obtained by nonlinear renormalization of the advective fluxes, Mon. Wea. Rev., 117, 1006-1015.

———(1992) Monotone flux limitation in the area-preserving flux-form advection algorithm, Mon. Wea. Rev., 120, 2592-2602.

Brost, R. A., P. L. Haagenson, and Y.-H. Kuo (1988) The effect of diffusion on tracer puffs simulated by a regional scale Eulerian model, J. Geophys. Res., 93(D3), 2389-2404.

Chang, J. S., R. A. Brost, I. S. A. Isaksen, S. Madronich, P. Middleton, W. R. Stockwell, and C. J. Waleck(1987) A three-dimensional Eulerian acid deposition model : Physical concepts and formulation, J. Geophys. Res., 92(D12), 14681-14700.

Davies, H. C.(1976) A lateral boundary formulation for multi-level prediction models, Quart. J. Roy. Meteorol. Soc., 103, 225-245

Draxler, R. R., J. L. Hefftner, and B. J. Stunder (1988) Across North America Tracer Experiment(ANATEX) Comprehensive plan, Report on meeting on the assessment of the

meteorological aspects of the third phase of EMEP, WMO report NO. 48, Appendix E, 1-25.

Eliassen, A., and J. Saltbones(1983) Modeling of long-range transport of sulphur over Europe : A two-year model run and some model experiments, Atmos. Environ., 17(8), 1457-1474.

Ferber, G. L., J. L. Hefftner, R. R. Draxler, R. J. Lagomarsino, F. L. Thomas, R. N. Dietz, and C. M. Benkovitz(1986) Cross-Appalachian Tracer Experiment(CAPTEX '83), Final Report, Environ. Res. Lab., Silver Spring, Md., Tech. Memo. ERL ARL-142, 60pp.

Kistler, R. E.(1974) A study of data assimilation techniques in an autobarotropic, premitive equation, channel model, M. S. thesis, Penn. State Univ., 84B.

Kotamarthi, V. R. and G. R. Carmichael(1990) The long range transport of pollutants in the Pacific rim region, Atmos. Environ., 24A, 1521-1534.

Lee, I. Y.(1987) Numerical simulations of cross-Appalachian transport and diffusion, Bound.-Layer Meteor., 39, 53-66.

Mesinger, F. and A. Arakawa(1976) Numerical methods used in atmospheric models, GARP Publ. Ser., 17, 1-64.

Prather, M. J.(1986) Numerical Advection by Conservation of Second-order Moments, J. Geophys. Res., 91, 6671-6681.

Shim, S. G., Y. P. Kim, D. G. Lee, and S. Y. Cho (1993) A study on the Development and Application of Air Dispersion Models and Acid Precipitation Models(III), KIST Report, UCN875(6)-4679-6, 179pp.

Smolarkiewicz, P. K.(1983) A simple positive definite advection scheme with small implicit diffusion, Mon. Wea. Rev., 111, 479-486.

Tremback, C. J., and R. Kessler(1985) A surface temperature and moisture parameterization for use in mesoscale numerical models, Report on 7th conference on numerical prediction June 17-20, 1985, Montreal, Quebec, Canada, AMS.

————, G. J. Tripoli, and W. R. Cotton(1985) A regional scale atmospheric numerical model including explicit moist physics and a hydrostatic time-split scheme, Preprints, 7th Conference on Numerical Weather Prediction, June 17-20, 1985, Montreal, Quebec, AMS.

Tripoli, G. J., and W. R. Cotton(1982) The Colorado State University three-dimensional cloud/meso-scale model. Part I : General theoretical framework and sensitivity experiments, J. de Rech. Atmos., 16, 185-219.

CAPTEX 자료에 나타난 추적물 농도 분포의 수치 모사

연세대학교 천문대기과학과·지구환경연구소
김승범, 이태영

초 록

지역 규모 대기 모형과 결합된 오일러 장거리 수송 모형이 제시되었다. 이 모형을 Cross-Appalachian Tracer Experiment (CAPTEX)의 2개 사례에 나타난 추적물 농도 분포 모사에 적용하였다. 기상장은 CSU RAMS에 4차원 자료 동화 기법을 도입하여 도출하였고, 추적물 수송은 오일러 확산 모형으로 계산된다.

4차원 자료 동화 기법을 포함한 대기 모형은 관측과 잘 일치하는 기상장을 도출하였으며, 장거리 수송 예측에 이용될 다양한 기상 자료의 도출을 위한 매우 적절한 도구가 될 수 있음을 보였다. 이 연구에서 개발된 수송 모형은 관측 농도 분포가 복잡한 구조를 보인 사례에 대해서는 부분적인 성공을 거두었으나, 대체로 관측된 추적물 수송을 유사하게 모사하였다. Bott's 2nd-order scheme을 사용한 결과는 Bott's 4th-order scheme을 사용하고 명시적인 수평 확산을 증가시킨 경우와 유사한 수행 능력을 보였다. 이 대기 모형과 수송 모형은 상세한 구름 및 화학 과정들을 고려한 산성 침적 모형의 훌륭한 기본 틀이 될 수 있을 것으로 생각된다.